Journal of Colloid and Interface Science 386 (2012) 16–27

Contents lists available at SciVerse ScienceDirect

Journal of Colloid and Interface Science

www.elsevier.com/locate/jcis

Dielectric analysis of multi-layer structure of nanofiltration membrane in electrolyte solutions: Ion penetrability, selectivity, and influence of pH

Kongshuang Zhao *, Jingjin Jia

College of Chemistry, Beijing Normal University, Beijing 100875, China

ARTICLE INFO

Article history:
Received 23 February 2012
Accepted 3 July 2012
Available online 22 July 2012

Keywords:
Nanofiltration membranes
Dielectric spectroscopy
Donnan equilibrium
Solvation energy
Ion penetrability

ABSTRACT

Dielectric measurements were carried out on the systems composed of NF membrane and dilute electrolyte with different concentration and 0.1 mol/m^3 solutions with different pH. Double dielectric relaxations were observed in frequency range of 40 Hz–10 MHz. The two relaxations are caused by the interfacial polarization between the membrane and solution and the multi-layer structure of the membrane. A triple-layer-plane model was adopted to analyze the dielectric spectra. It was found that the electric properties change with the concentration and pH of electrolyte solution. The fixed charge density was estimated, and the ion permeations in both sub-layers were compared. The results were interpreted based on Donnan equilibrium and dielectric exclusion principle. The two sub-layers were then confirmed as a dense active layer and a porous support layer, respectively. Special attention was paid on the permeability and selectivity of the active layer. The results indicated that the active layer has the different solvation energy barrier for divalent and monovalent co-ion and the selectivity for co-ion penetrating into it. The permeability of the porous support layer, however, has no selectivity for different electrolytes, and electrolyte easily passes through this sub-layer. Moreover, the pH dependence of the dielectric spectra was also analyzed.

1. Introduction

The nanofiltration (NF) membrane commonly used in liquid phase separation is a key component of the NF technique. The separation efficiency of the NF process mainly depends on the electrical and/or structural characteristics of the NF membranes as well as on the chemical nature of the treated solutions. Therefore, it is foundationally significant to study the transport performance, including ion penetrability and selectivity. Meanwhile, these researches have potential significance for interpreting some elementary phenomenon occurring in membrane/solution interface. For these reason, the research on the basal phenomenon related to practical membrane process has attracted increasing attention over recent years [1–3]. Numerous papers about the separation properties of NF membrane have been published, being devoted to understand the separation mechanism, the penetrability, and the selectivity [4–6].

In the case of uncharged molecules separation, steric hindrance is considered to be responsible for the penetrability and selectivity of the molecules in NF membrane [7], whereas for charged species, both steric hindrance and electrostatic interactions between membrane and solutes may play dominant roles [8–10]. The ion selectivity through NF membrane is normally determined by the valence of the co-ion, but lesser extent by the valence of the counter-ion. Therefore, it is crucial to get the parameters that show the effective structural features (thickness of constituent layers and porosity) and electrical properties of NF membrane (volume charge density) for understanding the details of membrane transport mechanism.

Although scanning electron microscopy (SEM), X-ray photoelectron spectroscopy (XPS), atomic force microscopy (AFM), etc., can give us information on the surface morphology of dry membranes, for example, surface roughness, mean pore size and porosity distribution, and membrane thickness [11–13], these characteristics of the membrane in dry state cannot represent the properties of the membranes under working conditions (e.g., soaked in solutions). It is the characteristics under working conditions that are more closely related to membrane performance and the separation mechanism. Another method usually adopted to study the electrical properties of membrane soaked in solution is measuring membrane potential, which, however, only gives information on surface charges of the whole membrane [14,15]. For the NF membranes composed of multi-layer, this method is incapable of detecting the properties of inner structure of the membranes. Furthermore, the interpretation of the membrane potential is complex, since it is a non-monotone function with respect to the charge density and the correction for the surface conductance by using the equations available in the literature can lead to different results [16]. Therefore, these conventional measurements are not effective to

* Corresponding author. Fax: +86 1058802075.
E-mail address: zhaoks@bnu.edu.cn (K. Zhao).

0021-9797/$ - see front matter © 2012 Elsevier Inc. All rights reserved.
http://dx.doi.org/10.1016/j.jcis.2012.07.022

Nomenclature

C	capacitance
G	conductance
C^*	complex capacitance
G^*	complex conductance
f	frequency
c	concentration
$M^{(x+)}$	cation
$A^{(y-)}$	anion
C_x^m	the concentration of the fixed charge in membrane
z_i	valence of ion i
a_i	radius of ion i
r_p	the radius of membrane pore
L	the distance between two electrodes
S	the area of parallel plate capacitor
d	membrane thickness
e	electronic charge (C)
ΔW_i	Born solvation energy barrier
f_0	the characteristic frequency
ΔC_l	the relaxation strength of the low frequency relaxation ($=C_l - C_m$)
ΔC_h	the relaxation strength of the high-frequency relaxation ($=C_m - C_h$)
C_B^m	the concentration of anion in membrane layer b
C_B	the concentration of anion in bulk solution
D	the diffusion coefficient
Z_A	the charges of cation (counter-ion)
Z_B	the charges of anion (co-ion)

Greek letters

ε	permittivity
ε_0	permittivity of vacuum (8.8541×10^{-12} F/m)
τ	relaxation time
β	Cole's parameter

Subscripts

a	solution phase
b	the layer b of membrane
c	the layer c of membrane
t	theoretical value
e	experimental value
w	solution phase
m	membrane phase
x	charge numbers of cation $M^{(x+)}$
y	charge numbers of anion $A^{(y-)}$
b	bulk
p	membrane pore
l	low frequency
m	middle frequency
h	high frequency

predict the transport mechanism and to evaluate the distribution of charged species in membrane.

Dielectric spectroscopy (DS), as a noninvasive method, has been successfully used to acquire electrical and structural parameters of heterogeneous systems [17,18]. In practical separation processes, because membrane and electrolyte solution form a heterogeneous system containing multiple phase interfaces, Maxwell–Wagner interfacial polarization concept and theoretical formulas are suitable to analyze the dielectric spectra. A number of dielectric studies on different types of membranes by means of DS method (or electrical impedance spectra) have been reported [19–26]. Most of these studies took the membranes as a homogeneous phase to explore special phenomena at the membrane-solution interface, such as water splitting, fouling, and concentration polarization. However, it is well known that NF membranes are composed of two elements (a thin and dense active layer, often called skin layer, and a thick and porous support layer) [27], and the ion permeability through the membranes is determined mainly by the electrical properties of the skin layer and porosity of the membrane [28,29]. In other words, it is normally believed that the selectivity of a membrane and solute fluxes are controlled by the skin layer. Therefore, obtaining information the electrical and structural information on each sub-layer of the membrane, especially skin layer, is significant. On the other hand, because the permeation properties of membrane are strongly dependent on its compactability, that is, pore structure as well as membrane materials, the geometric parameters of each layer related to the ion permeability are also rather important. Moreover, fixed charge density of each layer is very useful for understanding the separating mechanism. To sum up, the characteristics of both sub-layers can provide valuable information on ion permeability and selectivity in NF membrane performance. The dielectric analysis based on an idealized electrical model can be used to achieve above purpose [30–33]. In our previous studies, the dielectric and electrical parameters of sub-layer in asymmetric nanofiltration membrane, that is, permittivity and conductivity, fixed charge content of the sub-layer, were estimated by the dielectric analysis method [33].

In this work, dielectric measurements were carried out for the systems composed of a NF membrane and dilute solutions of various electrolytes with varying concentrations. In order to describe the dielectric behavior of the systems under varying the concentration and the species of electrolyte, and pH of solution, we amended the model proposed previously by us and calculated the phase parameters in a new model, which presents a makeup of solution-membrane (with two sub-layers)-solution. The results were interpreted based on the Donnan equilibrium principle. Furthermore, the structural feature of the membrane and the ion permeability and selectivity of each layer in the membrane were discussed in detail. Especially, the selectivity of various salt solutes through the effective separation layer (i.e., active layer) of NF membrane was evaluated. In addition to this, the influence of pH of the solution on the membrane structure and solute permeability was also investigated. The 1–1 type and 1–2 type electrolytes were used to study their transport performance (permeability and selectivity) through the each sub-layer of NTR7450 membrane.

2. Theoretical background

2.1. Electrical model and analysis method

For a heterogeneous system comprised of the NF membrane and electrolyte solutions at both sides (see Fig. 1), the dielectric behavior can be readily interpreted with the Maxwell interfacial polarization theory. Because the whole membrane and solution domains have different electrical properties, when an electric field is applied to the system, spatial charges accumulate on the interfaces between the membrane and solution, leading to interfacial polarization [34]. Dielectric measurements give relaxation spectrum whose pattern (the number or distribution of relaxation) will change with the complication of systems [35].A triple-phase-plane model shown in Fig. 1 was adopted to calculate the apparent capacitance and conductance of each sub-layer in the membrane. From the dielectric point of view, Fig. 1a can be represented in

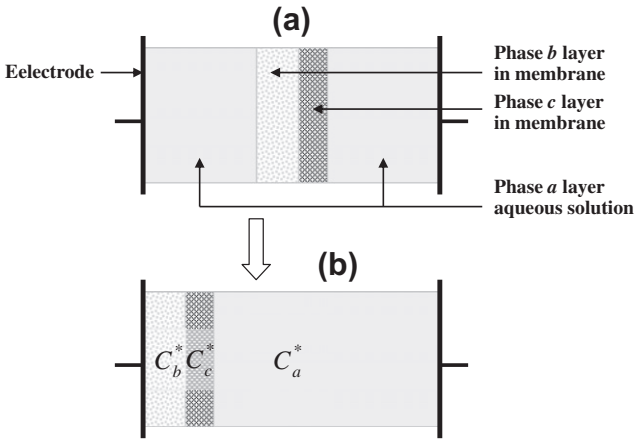

Fig. 1. Schematic diagram of the measured system (a) and its equivalent dielectric model (b). The system is composed of three phases with different complex capacitance, that is, aqueous solutions (phase a), C_a^*, layers in the membrane (phases b and c), C_b^* and C_c^*, respectively.

the form of Fig. 1b, that is, the solution phases in both sides of the membrane are considered as one phase because they are the same concentration electrolyte solution. Therefore, the present system can be considered to be composed of three constituent phases with different complex capacitances C_a^*, C_b^*, and C_c^*, corresponding to the solution phase *a*, the sub-layer *b*, and sub-layer *c* of the NF membrane, respectively. Fig. 2 represents the equivalent circuit to describe the dielectric spectra given by measuring the system of Fig. 1. And the equivalent circuit is associated with solution phase indicated by one sub-circuit and NF membrane consists of two sub-circuits, one for each layer, which allows the electrical and structural characters of dense and porous layers. The complex capacitance C^* and conductance G^* of the whole system (Fig. 1a or b) considered as a series combination of three sets of lumped capacitance and conductance as shown in Fig. 2a, and they are measured as the function of frequency. The formula representing the complex capacitance $C^*(f)$ is given as follows:

$$\frac{1}{C(f)^*} = \frac{1}{C_a^*} + \frac{1}{C_b^*} + \frac{1}{C_c^*} \tag{1}$$

The complex capacitance is defined as

$$C^*(f) = C(f) + \frac{1}{j2\pi f} G(f) \tag{2}$$

By dielectric measurements, we can obtain complex capacitance $C^*(f)$ of the entire system, which contains two variables, capacitance $C(f)$ and conductance $G(f)$, both depending on measuring frequency *f*. The complex capacitance $C^*(f)$ and complex conductance $G^*(f)$ is related in terms of the following equation:

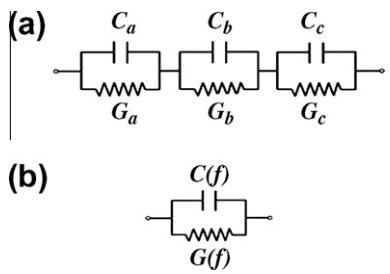

Fig. 2. (a) Circuit model to simulate a three layer structure composed of layer *a*, layer *b* and solution and (b) equivalent capacitance $C(f)$ and conductance $G(f)$ for the whole measuring system.

$$j\omega C^*(f) = G^*(f) \tag{3}$$

and

$$C_i^* = C_i + \frac{1}{j2\pi f} G_i, \quad i = a, b, c \tag{4}$$

where *f* is the frequency of the applied ac voltage, and *j* is the imaginary unit, defined as $j = \sqrt{-1}$. The C_i and G_i are capacitance and conductance of constituent phase *i* in the whole system. The dielectric spectrum of the NF membrane-solution system can be calculated with Eqs. (1)–(4) by introducing the values for the electric parameters (capacitance and conductance) of each constituent phase, C_a, G_a, C_b, G_b and C_c, G_c.

2.2. Determination of phase parameters from dielectric spectra

According to the numerical calculation method proposed by us[30], the electrical parameters, expressed shown in Fig. 2a, that is, the capacitances and conductances of the constituent phase, can be calculated by using the dielectric parameters determined from the spectra. However, because the dielectric relaxation in our systems is not Debye type, the calculation results exhibited a larger error. Therefore, we adopted a method of fitting dielectric data to Eq. (1) to obtain phase parameters. Therefore, to acquire the values of electric parameters of each phase, the least-squares method is employed to analyze the dielectric spectra, based on Eqs. (1)–(4). The best fitting is acquired when ξ reaches a minimal value. ξ is expressed as

$$\xi = \sum_{i=1}^{N} [(C_e'(f_i) - C_t'(f_i))^2 + (C_e''(f_i) - C_t''(f_i))^2] \tag{5}$$

where $N = 80$ is the number of the applied frequencies, f_i is *i*th measuring frequency, the subcript *t* and *e* refers to the calculated values using Eqs. (1)–(4), and *e* denotes the observed dielectric data; The C' and C'' represent the real part and imaginary of the complex capacitance C^* of the whole system shown in Eqs. (1) and (2). The fitting gives the values of C_a, G_a, C_b, G_b and C_c, G_c, which represent the capacitance and conductance of solution phase, and two sub-layers of the NF membrane, respectively, as described above.

2.3. Basic principles of ion permeation of membrane

It is generally recognized that the separation mechanism of the NF process is related to electrostatic partitioning effects between the charged membrane and the external solutions, or electrostatic interaction. Therefore, the Donnan equilibrium (or Donnan exclusion) and dielectric exclusion are usually used to interpreted these issues [36]. According to Donnan equilibrium, the ion selectivity of membrane is mainly determined by the valence of the co-ion and to a lesser extent by the valence of the counter-ion.

The quantity of fixed charge in membrane is also an essential parameter for estimating the separation mechanism. In the light of the Donnan equilibrium principle, when a charged membrane is equilibrated with *MyAx* type electrolyte solution, the concentration of cation $M^{(x+)}$ and anion $A^{(y-)}$ in membrane and solution have the following relation:

$$\left(\frac{C_{M^{x+}}^w}{C_{M^{x+}}^m}\right)^x = \left(\frac{C_{A^{y-}}^m}{C_{A^{y-}}^w}\right)^y \tag{6}$$

where *C* is concentration (mol/m^3), superscripts *w* and *m* denote the solution and membrane phase, and *x* and *y* are the charge numbers of the cation $M^{(x+)}$ and anion $A^{(y-)}$, respectively. For the system composed of the membrane with negative fixed charges and *MyAx* type electrolyte solution, the condition of electroneutrality in the two

phases of membrane and solution can be given by following equations

$$xC^m_{M^{x+}} = yC^m_{A^{y-}} + C^m_x \tag{7}$$

$$xC^w_{M^{x+}} = yC^w_{A^{y-}} \tag{8}$$

where C^m_x is the concentration of the fixed charge in membrane. The solution of the simultaneous Eqs. (6)–(8) gives the expressions for concentrations of cation $M^{(x+)}$ and anion $A^{(y-)}$ in membrane[32]. For a mono–monovalent electrolyte, they are

$$C^m_{M^+} = \frac{\sqrt{(C^m_x)^2 + 4C^2} + C^m_x}{2} \tag{9a}$$

and

$$C^m_{A^-} = \frac{\sqrt{(C^m_x)^2 + 4C^2} - C^m_x}{2} \tag{9b}$$

where C is the concentration of the electrolyte in solution. For a di–monovalent electrolyte, the expressions are

$$C^m_{M^+} = 2\left(\sqrt[3]{\left(\frac{C^3}{2} - \frac{(C^m_x)^3}{216}\right) + \sqrt{\frac{C^6}{4} - \frac{(C^m_x)^3 C^3}{216}}} + \sqrt[3]{\left(\frac{C^3}{2} - \frac{(C^m_x)^3}{216}\right) - \sqrt{\frac{C^6}{4} - \frac{(C^m_x)^3 C^3}{216}}}\right) - \frac{2C^m_x}{3} \tag{10a}$$

and

$$C^m_{A^-} = \sqrt[3]{\left(\frac{C^3}{2} - \frac{(C^m_x)^3}{216}\right) + \sqrt{\frac{C^6}{4} - \frac{(C^m_x)^3 C^3}{216}}} + \sqrt[3]{\left(\frac{C^3}{2} - \frac{(C^m_x)^3}{216}\right) - \sqrt{\frac{C^6}{4} - \frac{(C^m_x)^3 C^3}{216}}} - \frac{C^m_x}{6} \tag{10b}$$

By means of Eqs. (10a) and (10b), the values of C^m_x in membrane can be calculated[32].

However, Donnan equilibrium is not sufficient to explain the ion permeation phenomenon of charged membrane. Therefore, dielectric exclusion is usually adopted to couple with the Donnan equilibrium to describe ion permselective of membrane. The dielectric exclusion is caused intrinsically by the difference between the permittivity of solution phase and membrane phase (polymeric matrix). Thus, the electrostatic interactions between the ions in solution and the polarization charges are induced by the ions on the polymeric matrix surface. On the other hand, because the sign of polarization charges and ions in solutions are the same, the interactions bring about an additional rejection effect. Moreover, the rejection effect will change with solvent permittivity in membrane pore; this is because when ions transfer from bulk solution of high permittivity to membrane pores of low permittivity, dielectric exclusion effect occurs. More specifically, when the solvent permittivity in the membrane pore decreased, the rejection effect will be enlarged [37]. On the basis of the above principle, Hagmayer [38] and Bowen [39] proposed empirical approaches to account for the change of the permittivity between the pores and bulk solution: an equation that indicates the change of the electrostatic free energy of an ion between in the solution and in the membrane pore was derived based on the Born equation in which only the permittivity of whole membrane was considered [40]:

$$\Delta W_i = \frac{z_i^2 e^2}{8\pi\varepsilon_o a_i}\left(\left(\frac{1}{\varepsilon_p} + \frac{0.393}{r_p/a_i\varepsilon_m}\left(1 - \frac{\varepsilon_m}{\varepsilon_p}\right)^2\right) - \frac{1}{\varepsilon_b}\right) \tag{11}$$

where z_i and a_i are valence and radius of ith ion, respectively, r_p is the radius of membrane pore, ε_b, ε_m, and ε_p are the permittivity of bulk, membrane and membrane pore, respectively. The ε_b and ε_m can be calculated by the following expressions: $\varepsilon_b = C_w(L/\varepsilon_0 S)$, $\varepsilon_m = C_m(d/S\varepsilon_0)$ (L, S are the parameters related with measuring cell will be presented in next section and d is the membrane thickness). The value of pore permittivity ε_p in Eq. (11) is difficult to obtain from experiments. Nevertheless, an approximation, the difference of free energy, namely Born solvation energy barrier, can be calculated by using following Born equation [41]:

$$\Delta W_i = \frac{z_i^2 e^2}{8\pi\varepsilon_0 a_i}\left(\frac{1}{\varepsilon_m} - \frac{1}{\varepsilon_b}\right) - \frac{z_i^2 e^2}{4\pi\varepsilon_0\varepsilon_m d}\ln\left(\frac{2\varepsilon_b}{\varepsilon_m + \varepsilon_b}\right) \tag{12}$$

The meanings of the symbols in Eq. (12) are the same as those in Eq. (11). However, estimating the permittivity of wet membrane is still difficult as stated in introduction. For this reason, one of the main purposes of this work is to get the permittivity of the membrane in electrolyte solution.

3. Experimental

3.1. Nanofiltration membrane

The nanofiltration membrane used in this work is NTR7450, which was kindly supplied by Nitto Denko Co., Japan. This membrane consists of a supporting fabric and an effective layer. The effective layer includes two sub-layers made from polyester and sulfonated polyether sulfone, respectively, one of which will play a key role in the separation process. The membrane is negatively charged in solution as a result of partial dissociation of the sulfonic groups ($-SO_3H$) in polymeric matrix of the membrane. The supporting fabric was peeled off before dielectric measurements. The thickness of the membrane without the fabric (fully swollen in electrolyte solution) is about 120 μm, and it was measured with a micrometer. A pretreatment of the membrane was carried out before measurements: first, the membrane without fabric was rinsed with ethanol and distilled water in turn to remove organic impurities, and then, it was immersed in distilled water for 24 h.

3.2. Dielectric Measurements

The dielectric measurements were carried out over a frequency range of 40 Hz–10^7 Hz using a precise impedance analyzer (Agilent Technologies) controlled by a personal computer. The membrane was sandwiched between a pair of cylindrical chambers, which were filled with same electrolyte solution, as shown in Fig. 1 and described in literature [30]. The electrodes attached to the chambers form a parallel plate capacitor with an area S of 3.14 cm^2. The cell constant (S/L) is 2.414 cm (L is the distance between two electrodes).The measuring systems in this work are composed of the same membranes and four electrolyte solutions, such as NaCl, $NaNO_3$, Na_2SO_4, and Na_2CO_3. The concentrations of these electrolytes vary from 0.05 to 10 mol/m^3. The dielectric measurements were also carried out for the systems (membrane and NaCl, $CaCl_2$, and Na_2SO_4 solutions, respectively) with varying pH from 4 to 10 under 0.1 mol/m^3. Before measurements, the membrane was allowed to immerse in the solution for 15 min to make it equilibrate with the solution. All of the dielectric measurements were repeated three times and the results showed good reproducibility. All measurements were performed between 17 ± 1 °C, and all the experimental data were subjected to certain corrections for the errors arising from residual inductance due to the cell assembly [42].

4. Result and discussion

4.1. Analysis for the dielectric spectra with varying concentration

4.1.1. Dielectric spectra

Fig. 3 shows a three dimensional representations for the concentration dependence of the dielectric spectra for the NF membrane and NaCl solution system in the concentration range of 0.05–10 mol/m^3. This dielectric spectrum shows a definite dielectric relaxation around 20 KHz and another ambiguous relaxation at about 1 kHz. Though the low-frequency relaxation is not legible, it can be confirmed distinctly by the complex plan plots of the same data, as shown in Fig. 4. From Fig. 3, it can be seen that the high-frequency relaxation shifts obviously to the lower frequency side as the concentration decreases (as indicated by arrows). This dielectric behavior can be defined as a typical feature of M-W interfacial polarization mechanism [43].

4.1.2. Estimation of dielectric parameters

To examine the characteristics of dielectric spectra and to explore the origin of these relaxations, it is necessary to obtain the relaxation parameters (dielectric parameters) characterizing the dielectric spectra. For this purpose, the capacitance curves of dielectric spectra (Fig. 3a) were represented by a sum of two sub-relaxations of Cole–Cole type [44]

$$C = C_h + \frac{(C_l - C_m)\left[1 + (f/f_{0l})^{\beta_l}\cos\left(\frac{\pi}{2}\beta_l\right)\right]}{1 + 2(f/f_{0l})^{\beta_l}\cos\left(\frac{\pi}{2}\beta_l\right) + (f/f_{0l})^{2\beta_l}} + \frac{(C_m - C_h)\left[1 + (f/f_{0h})^{\beta_h}\cos\left(\frac{\pi}{2}\beta_h\right)\right]}{1 + 2(f/f_{0h})^{\beta_h}\cos\left(\frac{\pi}{2}\beta_h\right) + (f/f_{0h})^{2\beta_h}} \quad (13)$$

where C_h, C_l, and C_m are the limit of the capacitance at high-, low-, and middle frequency, respectively. $(C_l - C_m)$ and $(C_m - C_h)$ are the magnitudes of the sub-relaxations (relaxation strength or dielectric increment) at low- and high-frequency, respectively. f is the measuring frequency, f_0 is the characteristic frequency, which is calculated from $f = 1/(2\pi\tau)$(τ is relaxation time), and $\beta(0 \leqslant \beta < 1)$ is the dispersion parameter of relaxation time. The fitting results provided the relaxation parameters, C_h, C_l, C_m, f_{0l}, f_{0h}, β_l and β_h. However, it is difficult to obtain the conductance parameters of dielectric spectra by fitting the conductance curves represented by Fig. 3b. In this work, the G_l was determined directly from the curves of $G - f$, G_h was estimated from the complex conductivity plane as illustrated in Fig. 5, and G_m was obtained from the plot of measured conductance against capacitance over whole frequency according to literature [30]. All the dielectric parameters obtained above are listed in Table 1. The characteristic relaxation frequency (f_{0l},f_{0h}) and the relaxation strength at low- and high-frequency relaxation ($\Delta C_l(= C_l - C_m)$, $\Delta C_h(= C_m - C_h)$) are plotted as function of the concentration of NaCl solution in Fig. 6. From Fig. 6, it can be seen that f_{0l} and f_{0h} increase linearly with different slopes as the concentration of NaCl increase as shown in Fig. 6a and b, implying their different relaxation mechanism. Moreover, it is obvious from Fig. 6 that there are similarities and differences between the relaxation strengths at low- and high-frequency: both of the two curves existed a turning point at about 1 mol/m^3 NaCl concentration, below this concentration, both ΔC_l and ΔC_h increase sharply with increasing concentration; above this concentration, ΔC_h levels off and ΔC_l increases slightly with increasing concentration. In addition, because the number of dielectric relaxation is equal to the number of interface for a heterogeneous according to Hanai et al. [35], the two relaxations can be considered to be caused by the interface polarization originated from two interfaces. Therefore, we assume that the two interfaces are the interface between the whole membrane and bulk solution, and the one between two sub-layers inside the membrane. It has been testified that the relaxation at higher frequency originates from the interface between the whole membrane and bulk solution [30,33,35], so the low-frequency relaxation can be believed to be caused by the two sub-layers with different electrical properties in the NF membrane.

4.1.3. Analysis of phase parameters

Based on the above analysis, the present system can be modeled as an electrolyte solution/layer *b*/layer *c* configuration in series, in conformity with that illustrated in Fig. 1b. For such configuration, an analysis method aiming to calculate numerically the constituent phase parameters has been developed [30]. However, because the data of low frequency itself in this work is not very accurate, it is difficult to calculate accurately phase parameters using this method. Therefore, the best fitting method introduced in Section 2.3 was adopted. The curve-fittings were performed by using Eq. (1). All the obtained phase parameters are shown in Table 2.

4.1.4. Electrical and structural properties of two-layers in membrane

The phase parameters obtained by analyzing the dielectric spectra (Table 2) showed that the capacitance of NaCl solution phase, C_a has an average value of 17.88 pF within the concentration range of 0.05–10 mol/m^3. According to the relation $C = \varepsilon_0\varepsilon(S/L)$, the permittivity of NaCl solution was estimated to be about 83.60, which is slightly higher than that of pure water at 18 °C. For $NaNO_3$, Na_2SO_4 and Na_2CO_3, their permittivity showed an approximate value between 81 and 83, being a reasonable scope. The conductance of NaCl solution, G_a, increases as concentration increases, which is be-

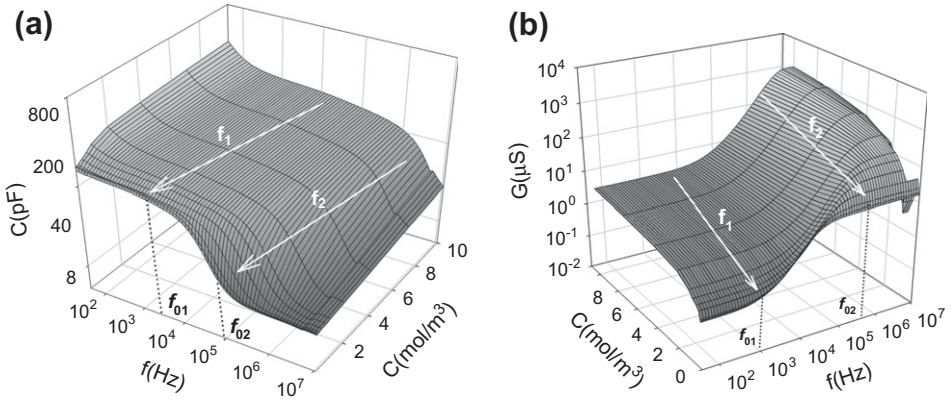

Fig. 3. Three-dimensional representations of concentration dependence of (a) the capacitance spectrum and (b) the conductance spectrum for system composed of NF membrane and NCl solution.

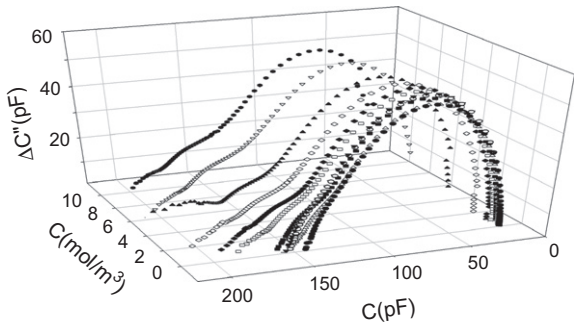

Fig. 4. Complex plan plots of capacitance for the data of NF membrane in NaCl solutions system, in which $\Delta C'' = (G(f) - G_l)/2\pi f$.

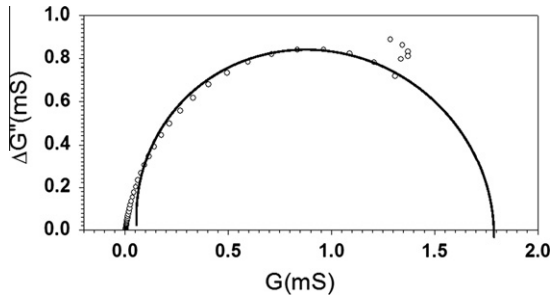

Fig. 5. Determination of G_h from a complex conductance G^*-plane plot[$\Delta G'' = 2\pi f(C - C_h), G$] of the data for the membrane in a 10 mol/m^3 NaCl solution.

cause the ions contribute to the electrical conductance. With regard to the capacitance and conductance of the two sub-layers (*b* and *c* phase), the magnitude of their values are obviously different, that is, $C_b \gg C_c$ and $G_b \ll G_c$ in the range of experimental concentration. This is due to the difference between the electrical and structural properties of the two sub-layers.To examine the electrical and structural characteristics of the *b* and *c* phase, the phase parameters of *b* phase and *c* phase, C_b, G_b, C_c, G_c, for the systems composed of membrane and NaCl, $NaNO_3$, Na_2SO_4 and Na_2CO_3 four kinds of electrolyte solutions respectively, were plotted as function of the concentration of corresponding electrolyte solutions in Fig. 7. By comparing Fig. 7a–c, the difference in capacitance between *b* phase and *c* phase for the case of four kinds of electrolyte solutions in experimental concentrations range can be clearly seen. On average, the values of C_b are 20–30 times larger than that of C_c, suggesting that the *b* sub-layer is relatively thin and corresponds to the effective separation layer. In contrast, not only $G_b < G_c$, but also the concentration dependences of G_b and G_c are different from each other as shown in Fig. 7b and d. Compared with G_c, G_b is smaller by two orders of magnitude, indicating that penetration of ions through layer *b* is more difficult than through layer *c*. This suggests that the structure of layer *b* is more compact. G_c increases approximately linearly with the electrolyte concentration, which is remarkably similar to the concentration dependence of G_a, and the values of G_c for 1–2 type electrolyte solution is always greater than that for 1–1 type as shown in the inset in Fig. 8d. In addition, on average, the slope of the straight line for 1–2 type electrolyte solution is 5.596×10^{-4} S m^3/mol, whereas that for 1–2 type, it is 2.402×10^{-4} S m^3/mol. On the other hand, the average slope for 1–2 type electrolyte and 1–1 type electrolyte is 6.173×10^{-4} S m^3/mol and 2.924×10^{-4} S m^3/mol, respectively, showing the behavior of electrical conduction in layer *c* is similar to that of electrolyte solution phase *a*. These results imply that the transport of ions in layer *c* is almost unimpeded by polymer matrix and is similar to that in solution, in other words, the layer *c* has high water permeability. This can also be proved by the fact that the C_c is nearly invariable in the experimental concentration range as shown in Fig. 7c. Therefore, it can be deduced that the layer *c* is a supporting layer with a porous, loosing structure. Concerning the conductance of layer *b*, G_b maintained a stable value in low concentration, but increased exponentially as the concentration increases when the concentration was far above certain value 0.4 mol/m^3 as shown in Fig. 7b, showing a typical behavior of ions getting through charged membrane layer described by Donnan equilibrium. Furthermore, this also indicated that the layer *b* may have fixed charges.

Though above analysis, the electrical and structural properties of phase *c* and phase *b* in the model illustrated in Fig. 1 have been determined. Therefore, we can confirm the NF membrane used in this work is composed of a porous supporting layer and a charged dense layer, that is, separation layer and the two layers correspond to the phase *c* and phase *b* in Fig. 1.

4.1.5. Ion permeability and selectivity of two-layers in membrane

Because the ratio of conductance G_c (porous support layer) and G_b (dense separation layer) to conductance G_a (bulk solution phase) respectively can be used to compare the ion transport performance in layers *c* and *b*, the plots of G_c/G_a and G_b/G_a against the concentration of electrolyte were made in Fig. 8. From Fig. 8a, what can be found is that the values of G_c/G_a for four kinds of electrolyte are all close to 1 in the experimental concentration range, being independent of the concentration and species of electrolyte of bulk solution. It can be therefore affirmed that the hindrance effect of matrix of layer *c* on ions is exceptionally small and electrolyte is easy to transport through this layer, and there is no selectivity for different electrolytes transporting through this layer *c*.

Concerning the separation layer *b*, the concentration dependence of G_b/G_a shown in Fig. 8b is distinctly different from the case of the layer *c*. G_b/G_a decreases sharply at very low concentrations, but it is independent of bulk concentration when the concentration

Table 1
Dielectric parameters for membrane in NaCl solutions with varying concentrations.

C (mol/m^3)	C_l (pF)	C_m (pF)	C_h (pF)	G_l (nS)	G_m (nS)	G_h (μS)	f_{0l} (kHz)	f_{0h} (kHz)	β_l	β_h
0.05	145.8 ± 0.5	118.0 ± 0.4	14.96 ± 0.05	242.6 ± 0.9	420.5 ± 2.4	16.02 ± 0.05	1.2 ± 0.1	21.4 ± 1.2	0.80	0.95
0.07	156.6 ± 0.5	123.6 ± 0.5	15.07 ± 0.06	219.7 ± 0.8	508.8 ± 2.2	18.34 ± 0.05	1.2 ± 0.1	23.6 ± 1.3	0.80	0.96
0.10	157.8 ± 0.6	125.9 ± 0.4	15.35 ± 0.06	254.7 ± 0.9	579.7 ± 2.2	24.87 ± 0.07	1.3 ± 0.1	30.8 ± 4.3	0.80	0.97
0.20	150.2 ± 0.5	124.7 ± 0.5	14.97 ± 0.06	419.2 ± 1.1	671.9 ± 2.3	43.55 ± 0.24	1.3 ± 0.1	56.0 ± 1.5	0.85	0.94
0.40	158.2 ± 0.5	132.9 ± 0.4	14.94 ± 0.05	531.2 ± 1.5	877.8 ± 3.5	86.44 ± 0.34	1.7 ± 0.1	98.8 ± 1.5	0.97	0.90
0.70	166.3 ± 0.6	132.7 ± 0.4	15.14 ± 0.07	661.3 ± 2.5	1367 ± 5	147.0 ± 0.9	4.4 ± 0.1	170.2 ± 5.8	0.89	0.93
1.00	170.6 ± 0.5	137.5 ± 0.5	15.35 ± 0.06	968.8 ± 3.7	1818 ± 5	208.4 ± 1.3	4.8 ± 0.2	229.6 ± 8.1	0.97	0.92
2.00	179.3 ± 0.6	141.3 ± 0.4	15.07 ± 0.05	1749 ± 4	3168 ± 10	417.5 ± 1.9	6.1 ± 0.2	422.6 ± 9.1	0.93	0.89
4.00	176.0 ± 0.6	138.6 ± 0.5	15.07 ± 0.05	2616 ± 5	1455 ± 5	805.2 ± 1.7	12.4 ± 0.2	872.6 ± 9.8	0.89	0.87
7.00	180.3 ± 0.6	138.5 ± 0.5	17.97 ± 0.04	3738 ± 6	7346 ± 14	1290 ± 5	19.8 ± 0.2	1389 ± 11	0.89	0.87
10.0	183.1 ± 0.5	138.4 ± 0.5	17.07 ± 0.05	4757 ± 7	9820 ± 16	1790 ± 5	20.9 ± 0.3	1969 ± 16	0.82	0.87

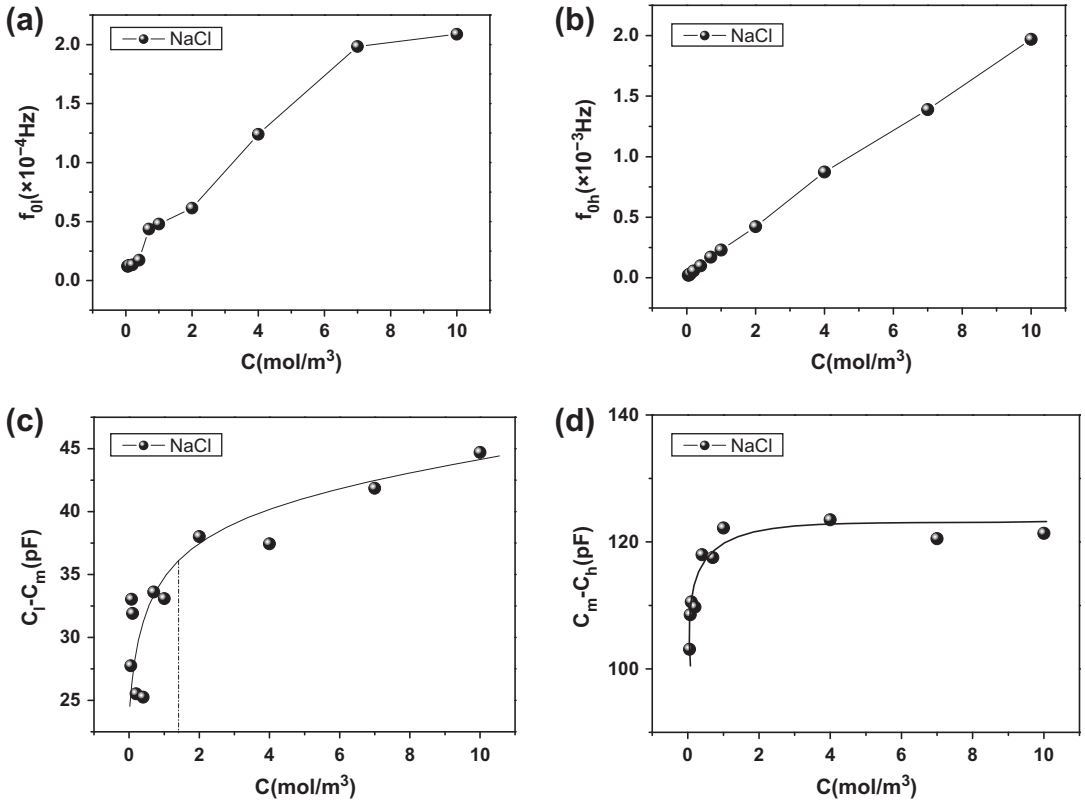

Fig. 6. Concentration dependence of relaxation parameters estimated by fitting the Eq. (14) to observed dielectric spectra (from the data in Table 1). (a) The characteristic frequency f_{0l} at low-frequency, (b) the characteristic frequency f_{0h} at high-frequency, (c)the amplitude of capacitance at low-frequency, and (d) amplitude of capacitance at high-frequency.

Table 2
Phase parameters for the system composed of membrane in NaCl solutions obtained by fitting Eq.(1) to dielectric spectra shown in Fig. 3.

C (mol/m^3)	C_a (pF)	C_b (pF)	C_c (pF)	G_a (μS)	G_b (μS)	G_c (μS)
0.05	18.04 ± 0.08	503.6 ± 2.5	17.01 ± 0.05	31.77 ± 0.15	4.906 ± 0.021	18.51 ± 0.05
0.07	18.29 ± 0.09	500.3 ± 2.3	17.05 ± 0.05	22.89 ± 0.12	4.951 ± 0.037	21.20 ± 0.05
0.10	18.19 ± 0.06	504.9 ± 2.1	17.38 ± 0.06	31.57 ± 0.15	5.315 ± 0.044	28.13 ± 0.06
0.20	18.01 ± 0.05	446.0 ± 2.4	16.95 ± 0.04	58.09 ± 0.25	4.839 ± 0.025	50.37 ± 0.15
0.40	18.04 ± 0.06	510.2 ± 2.5	16.79 ± 0.05	113.9 ± 0.5	7.008 ± 0.051	93.60 ± 0.53
0.70	17.93 ± 0.05	554.5 ± 2.6	17.04 ± 0.05	187.6 ± 1.0	18.54 ± 0.12	161.3 ± 0.8
1.00	17.71 ± 0.06	550.0 ± 2.5	17.23 ± 0.06	257.4 ± 1.2	21.28 ± 0.15	224.8 ± 1.1
2.00	17.85 ± 0.08	464.9 ± 2.5	16.83 ± 0.05	501.0 ± 3.1	24.10 ± 0.15	422.3 ± 2.5
4.00	17.62 ± 0.07	500.0 ± 2.3	16.88 ± 0.05	975.9 ± 3.9	51.58 ± 0.35	856.5 ± 3.5
7.00	17.52 ± 0.07	479.8 ± 2.4	20.61 ± 0.08	1770 ± 9	80.87 ± 0.51	1394 ± 9
10.0	17.52 ± 0.07	433.7 ± 2.5	19.44 ± 0.06	2420 ± 11	79.18 ± 0.45	1961 ± 10

is above a certain value. This can be interpreted by Donnan equilibrium as follows: when bulk concentration is far below the fixed charge concentration in layer *b*, the ions with opposite charge against the fixed charge in this layer, that is, counter-ion, are attracted into the layer or membrane phase due to electrostatic interactions, so the concentration of counter-ion in membrane phase is higher than bulk concentration, leading to G_b/G_a is high in low concentration. While with the increase in bulk concentration, G_b/G_a decreases until the fixed charge of layer *b* is neutralized, and then ion concentration in or out of the membrane phase will achieve a thermodynamic distribution equilibrium state.To evaluate thoughtfully the permeability and selectivity of the effective separation layer *b*, some parameters, such as the fixed charges concentration of layer *b*, ion concentration and diffusion coefficient in membrane phase, are necessary. According to Eqs. (9), (10) of Section 2.4, the fixed charge concentration and anion concentration in membrane phase were calculated and the results are listed in Table 3 and 4, respectively. The value of average fixed charge concentration, 1.381 mol/m^3 for this case, is essential to understand the ion permeability and selectivity of layer *b* because the magnitude of this value is associated with the retention effect of NF membrane on electrolyte. On the other hand, from the Table 4, it can be seen that the concentration of anion in membrane phase C_B^m is far less than that C_B in bulk solution at a concentration lower than 1 mol/m^3, and the value of C_B^m gradually approaches to that of C_B with increasing C_B. This reflects that the distribution of anion in membrane phase changes with the bulk concentration due to Donnan potential which essentially originates from the fixed negative charge in layer *b*.

In order to obtain more information on the ion penetrability and selectivity through the layer *b*, the diffusion coefficient *D* of anion, that is, co-ion in membrane phase for the systems composed of

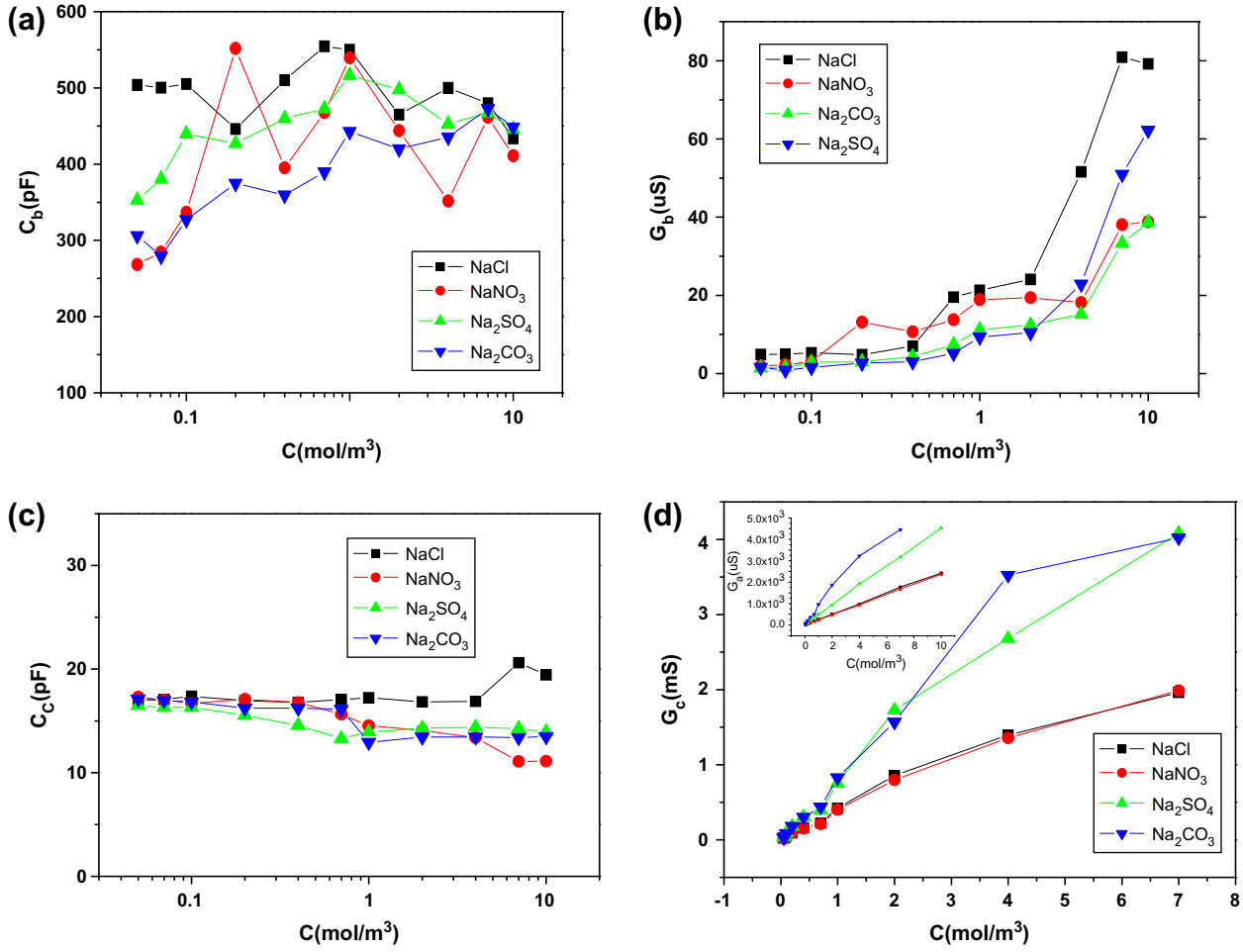

Fig. 7. Concentration dependence of phase parameters for the systems composed of NF membrane and NaCl, $NaNO_3$, Na_2SO_4, and Na_2CO_3 four kinds of electrolyte solutions, respectively. (a) Capacitance of *b* phase, (b) conductance of *b* phase, (c) capacitance of *c* phase, (d) conductance of *c* phase.

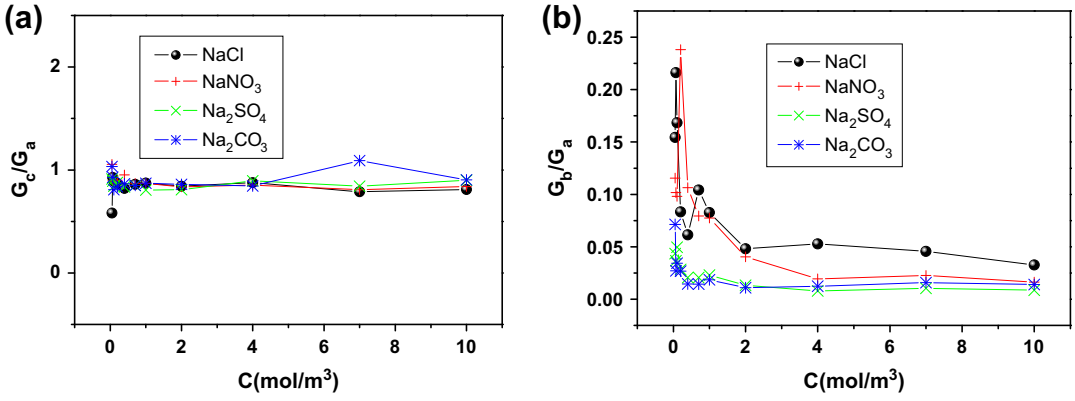

Fig. 8. The plots of the ratios G_c/G_a (a) and G_b/G_a (b) vs electrolyte concentration in four kinds of electrolyte solutions.

Table 3
The concentration of fixed charge in layer *b* of membrane.

	NaCl	$NaNO_3$	Na_2SO_4	Na_2CO_3	Average value
C_x^m (mol/m^3)	1.31	1.31	1.41	1.49	1.38

membrane and four kinds of electrolyte solutions, respectively, were calculated by using Eq. (14) [45] for AB type electrolyte, which was derived based on the Donnan equilibrium principle. The calculated results for varying concentrations are shown in Table 5 and Fig. 9.

$$D = \frac{C_B^m}{C_B} = \left(\frac{|Z_B|C_B}{|Z_B|C_B^m + C_x^m}\right)^{|Z_B|/|Z_A|} \quad (14)$$

where C_B^m and C_B are the concentration of anion in membrane layer *b* and in bulk solution, respectively, C_x^m is the concentration of fixed charges in the layer *b*, and Z_A and Z_B are the charges of cation (coun-

Table 4
The anion concentration (C_B^m (mol/m^{-3})) of layer *b* in varying concentration solutions.

C_B (mol/m^3)	NaCl	$NaNO_3$	Na_2SO_4	Na_2CO_3
0.05	0.0019	0.0019	–	–
0.07	0.0037	0.0037	–	–
0.1	0.0076	0.0076	–	–
0.2	0.030	0.030	–	–
0.4	0.11	0.11	0.26	0.25
0.7	0.30	0.30	0.53	0.52
1	0.54	0.54	0.81	0.80
2	1.44	1.45	1.78	1.77
4	3.40	3.40	3.72	3.71
7	6.38	6.37	6.64	6.62
10	9.37	9.37	9.54	9.53

Table 5
The diffusion coefficient (D) of anion in membrane phase.

C_B (mol/m^3)	Cl^-	NO_3^-	SO_4^{2-}	CO_3^{2-}
0.05	0.003807	0.03803	–	–
0.07	0.005322	0.05317	–	–
0.1	0.007581	0.07573	–	–
0.2	0.1491	0.1489	–	–
0.4	0.2809	0.2806	0.1701	0.1587
0.7	0.4334	0.4331	0.3199	0.3040
1	0.5401	0.5397	0.4334	0.4163
2	0.7245	0.7242	0.6488	0.6339
4	0.8494	0.8492	0.8156	0.8055
7	0.9107	0.9106	0.9086	0.9019
10	0.9365	0.9365	0.9521	0.9471

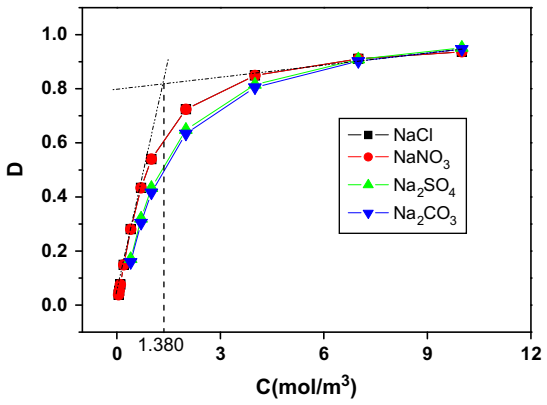

Fig. 9. The plots of the diffusion coefficient of anion in membrane phase vs the concentration of four kinds of electrolyte solutions.

ter-ion) and anion (co-ion), respectively.The concentration dependence of diffusion coefficient *D* in NaCl, $NaNO_3$, Na_2SO_4, and Na_2CO_3 solutions may be divided into two groups by the concentration of 1.380 mol/m^3 as shown in Fig. 9: *D* rises sharply within the concentration rang of 0–1.380 mol/m^3, and the increase slows down and gradually approaches to a stable value that is independent of the electrolyte concentration after 1.380 mol/m^3 with increasing concentration. This means that the obstruction of ion transporting through membrane is stronger when bulk solution is dilute, with the increase in bulk concentration the electrostatic exclusion weakens gradually because the fixed charges are neutralized by counter-ion, resulting in the ion penetration in membrane tended toward stability. By the calculated results and above analysis, it can be predicted that the transport of ion in membrane conforms to Donnan equilibrium, indicating that the membrane or layer *b* is electrically charged. On the other hand, from Fig. 9, it can be found that the values of diffusion coefficient *D* of anion in membrane for 1–1 type electrolyte, NaCl and $NaNO_3$, are greater than that for 1–2 type electrolyte, Na_2SO_4 and Na_2CO_3, at same concentration within the most concentration rang investigated. This suggests that divalent co-ion can hardly enter into the membrane, compared with monovalent co-ion, being attributed to the Donnan exclusion that the electrostatic effect is stronger for high charge ions. In other words, the layer *b* of NF membrane has certain preference for the permselectivity of monovalent co-ion through the membranes. It is also perceived from Fig. 9 that the two curves of 1–1 type electrolytes and the two curves for 1–2 type overlap with each other, this is because the Eq. (14) only considered the factor of electrostatic effect, but to other factors, such as steric hindrance and dielectric exclusion, had not been contained. It is undoubtedly that all possible factors which reflect the structural feature and the dielectric properties of membrane material should be considered to obtain more accurate information on the permselectivity of electrolyte through the membrane. Therefore, by using Eq. (13), the Born solvation energy barrier, which is the change of free energy of ion between bulk solution and membrane, for four systems composed membrane and four kinds of electrolyte solutions were calculated. In the calculations by Eq. (13), the permittivities of effective separation layer *b* in membrane and bulk solution were used, these values of permittivity are calculated beforehand respectively from the C_b and C_a in Table 2 according to the formulas $\varepsilon_b = C_b(d/S\varepsilon_0)$ (*d*, the thickness of layer *b*, 15 μm was adopted according to the literature[46]) and $\varepsilon_w = C_a(L/\varepsilon_0 S)$, and the values of ionic radius *a* for four kinds of anions adopted in calculation are from the literature[47]. These values with the solvation energy barrier ΔW obtained are listed in Table 6.

Table 6
Born solvation energy barrier of four systems calculated using Eq. (13) and the parameters in Eq. (13) for calculation.

	a (nm)	ε_b	ε_w	ΔW (eV)
NaCl	0.121	2.672	79.68	2.164
$NaNO_3$	0.129	2.213	79.18	2.585
Na_2SO^4	0.231	2.410	79.58	5.076
Na_2CO_3	0.202	2.087	79.41	6.836

From Table 6, it can be seen that the values of ΔW for 1–2 type electrolyte are bigger than that for 1–1 type. This also indicated that the hindrance of the effective reparation layer *b* to those ions with higher charge is larger than to lower charged ions, being in line with the feature of effective reparation layer *b* of the NF membrane [48].

4.2. Influence of pH on membrane permeability

4.2.1. Dielectric behavior under different pH media

Fig. 10 shows a three dimensional representations for the pH dependence of the dielectric spectra for the system composed of the NF membrane and 0.1 mol/m^3 NaCl solution. It is clearly seen from the complex plan plots of capacitance shown in Fig. 11 that this dielectric behavior also shows a dielectric spectrum with double relaxations as shown in Fig. 3. The relaxations parameters were gotten by fitting the dielectric spectra in the same way as described in Section 4.1.2. The pH dependence of the two relaxation strength of the two relaxations shows that they have respective change trends within the pH ranges of 4–10 as shown in Fig. 12. It is obvious that the relaxation strength of low-frequency $\Delta C_l (= C_l - C_m)$ in alkaline media is larger than that in acidic media, the relaxation strength of high-frequency $\Delta C_h (= C_m - C_h)$ remains virtually unchanged in experimental pH range. This result clearly indicates that the pH of solution changed the relaxation characteristics of low-frequency relaxation. On the other hand, as mentioned in

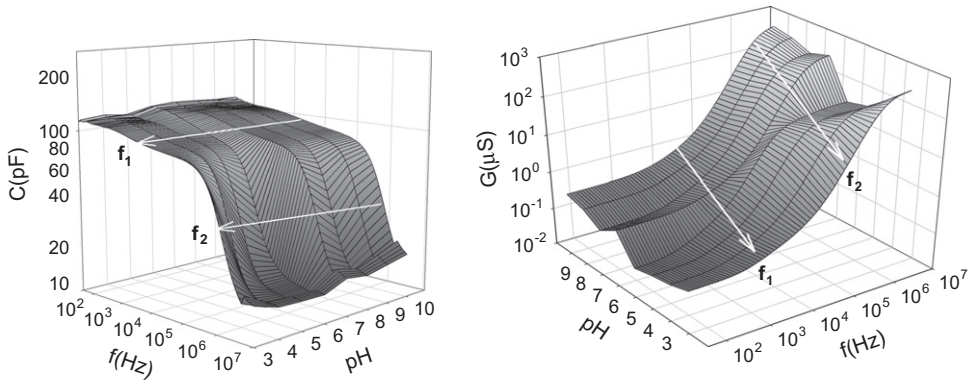

Fig. 10. Three-dimensional representations of pH dependence of (a) the capacitance spectrum and (b) the conductance spectrum for system composed of NF membrane and 0.1 mmol/L NCl solution.

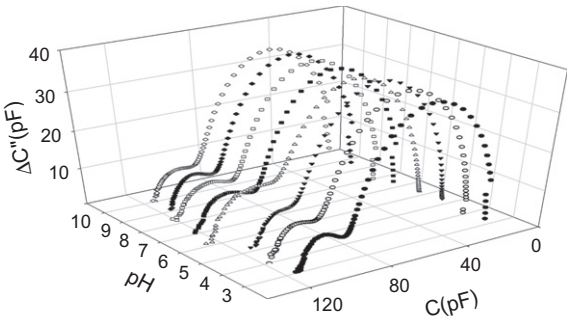

Fig. 11. Complex plan plots of capacitance for the data of NF membrane in 0.1 mol/m^3 NaCl solution at different pH, in which $\Delta C'' = (G(f) - G_l)/2\pi f$ and G_l is the low-frequency limit of conductance.

the previous part, the low-frequency relaxation is caused by the nonuniformity of the multi-layer membrane. Therefore, it may be decided that the acidity–alkalinity of electrolyte solution may changed the electrical or/and structural properties of the multi-layer membrane, which led to the change in capacitance of low-frequency relaxation.

In order to get more information on the electrical properties of two-layers inside the membrane, especially the permeability of effective reparation layer *b* when pH of the solution is changed, the method described in Section 4.1.3 is equally adopted to analyze the dielectric spectrum data of Fig. 10 and the phase parameters obtained under varying pH are listed Table 7.

4.2.2. Influence of pH on porous support layer of membrane

Fig. 13 shows the pH dependence of G_c/G_a. It is clearly from Fig. 13 that G_c/G_a approximately equal to 1, indicating that the conducting performance of ion in support layer *c* is similar to that in bulk solution. This therefore can be considered as that the layer *c* has loose structure and the pore size is big enough for ion to transport through it, being accordant with the speculation discussed in Section 4.1.4. Moreover, C_c has little change with the pH of bulk solution within the range of 4–10 pH as shown in Fig. 14. Therefore, it can be concluded that the pH of bulk solution has almost no effect on the electrical properties of the porous support layer *c*, and the permeability of the porous support layer *c* is not affected by pH of bulk solution.

4.2.3. Influence of pH on dense active layer of membrane

Fig. 15 shows the pH dependence of the ratio of G_c/G_a. It is obvious that the pH dependence of G_b/G_a is completely different from that of G_c/G_a. There is a point of inflexion at pH 6 for NaCl and $CaCl_2$ solutions and at pH 7 for Na_2SO_4, respectively, that is, the increment in G_b/G_a at neutral or weak acid region. These results implied that the structure of dense active layer *b* may change with pH of solution and the species of electrolyte. The variation of G_b/G_a with the pH may be due to the change of charge and can be interpreted from the chemical composition of the active layer *b* as follow: Since the layer *b* is mainly comprised of sulfonated polyether sulfone, the hydrogen ion H^+ on sulfonic groups can be released in solution because of the partial dissociation of the sulfonic group, and the degree of release will change with pH. When the pH decreases, that is, in acidic region, the release of H^+ will be restrained, whereas

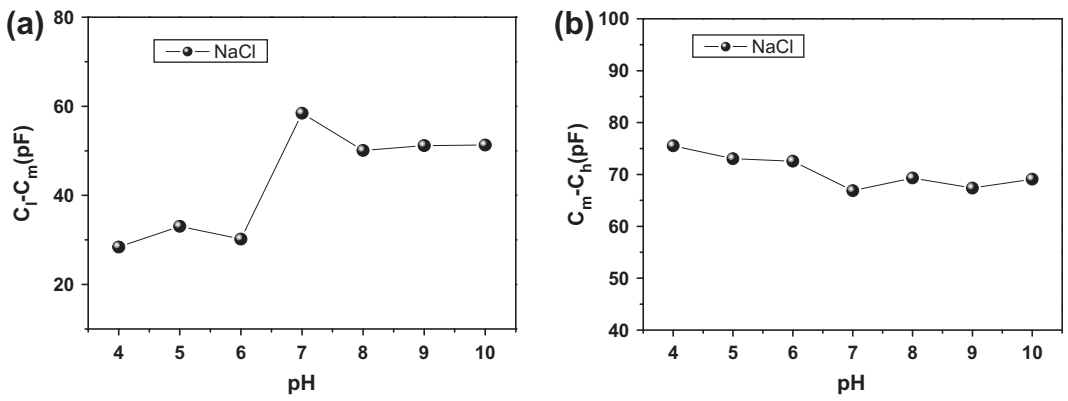

Fig. 12. pH dependence of capacitance increment of low-frequency, $\Delta C = C_l - C_m$ (a) and capacitance increment of high-frequency, $\Delta C = C_m - C_h$ (b) for the system composed of NF membrane and 0.1 mol/m^3 NaCl.

Table 7
The phase parameters of different pH calculated based on triple-phase-plane model for the system of the NF membrane in NaCl solution of 0.1 mmol/L.

pH	C_a (pF)	C_b (pF)	C_c (pF)	G_a (μS)	G_b (μS)	G_c (μS)
4	121.0	323.3	14.37	604.2	6.917	584.8
5	125.3	287.6	16.45	192.9	4.523	183.5
6	122.2	310.3	17.13	78.25	3.971	75.82
7	173.5	144.7	13.87	637.8	2.938	559.2
8	146.2	189.2	15.22	439.4	3.516	400.4
9	150.1	170.9	14.50	647.5	5.023	628.8
10	176.2	150.2	13.80	972.4	3.257	813.7

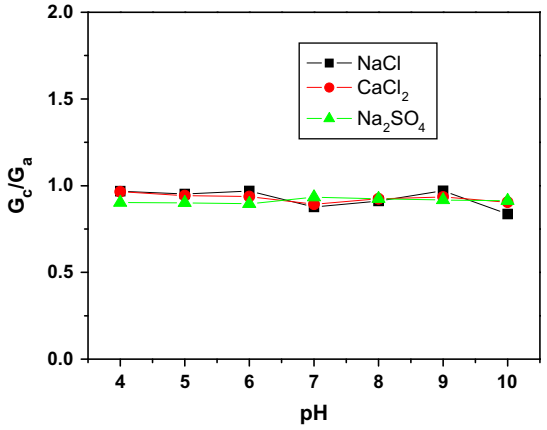

Fig. 13. Plots of ratio C_c/C_a of C_c–C_a against pH in NaCl, $CaCl_2$, Na_2SO_4 solutions.

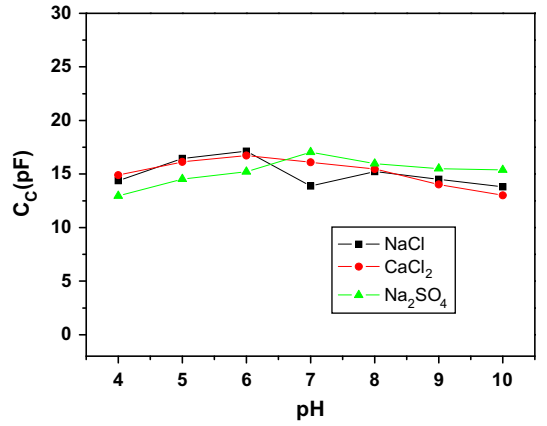

Fig. 14. pH dependence of capacitance of support layer *c* for NaCl, $CaCl_2$, Na_2SO_4 solutions.

when pH increases up to basic region, the H^+ will release completely. In other words, the quantity and state of fixed charge in the active layer *b* will change with pH too, resulting in the change of the difficulty degree for ion transport through the layer, this is similar to that has been reported [49].

Taking the system of NaCl and membrane, which is sensitive to pH, as an example, we analyze how the pH of bulk solution affects the migration of ions through the active layer *b*. Fig. 16 shows the pH dependence of capacitance of the active layer *b*, for NaCl and membrane system in the range of 4–10 pH. From this figure, it is clearly that the value of C_b at acid region is greater than that in basic region, being consistent with result of G_b/G_a shown in Fig. 15. According to these results, it may be concluded that some structural or/and electrical features of the membrane, especially the active layer *b*, were changed in acid region, resulting in the mobility of ions trough the membrane was facilitated. With increasing pH, the amount of fixed charges in the membrane increases, and the electrostatic exclusion between polymer chains in the membrane is enhanced [50]. As a result, the membrane pore becomes smaller and the ion transport is hindered and salt retentions are higher. This is in accordance with the conclusion of literature [14]. The Figs. 15 and 16 also show that for the G_b/G_a and C_b of divalent co-ion in 4-10 pH range, there is no significant difference between $CaCl_2$ and Na_2SO_4.

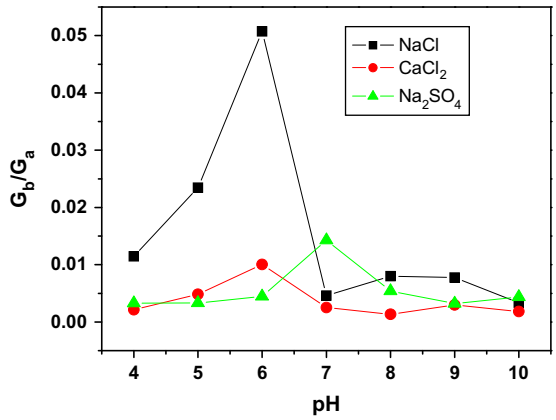

Fig. 15. Plots of ratio G_b/G_a of G_c–G_a against pH in NaCl, $CaCl_2$, Na_2SO_4 solutions.

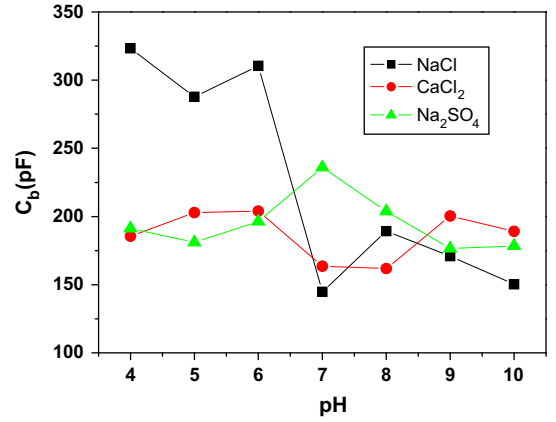

Fig. 16. pH dependence of capacitance of active layer *b* for NaCl, $CaCl_2$, Na_2SO_4 solutions.

5. Concluding remarks

The dielectric measurements were carried out for the systems composed of NTR7450 membrane and four electrolyte solutions, respectively, with varying concentration and pH. The double dielectric relaxation was observed for the four systems in the frequency range from 10 Hz to 40 MHz. Based on the simple three-phase circuit model, the dielectric spectra of these systems were analyzed systematically, and the electrical parameters inside the membrane were estimated. Furthermore, the results obtained from dielectric analysis were interpreted based on the Donnan equilibrium principle and the structural feature of the membrane and the ion permeability and selectivity of each layer in the membrane, especially, the effective separation layer (i.e., active layer), were discussed in detail. The two sub-layers were confirmed as a dense active layer and a porous support layer, respectively.

The distribution of the co-ion, that is, anion, in effective separation layer in different electrolyte solutions with varying concentration was calculated. Besides, the solvation energy barrier, which reflects the change of free energy of ion between bulk solution and the membrane, for four kinds of systems was also calculated. From these results, we concluded that the values of solvation energy barrier for 1–2 type electrolyte are larger than that for 1–1 type, showing the magnitude of energy rampart is related to the valence of the co-ion. On the other hand, by analyzing the pH dependence of dielectric parameters, some information on the structural change of dense active layer were also obtained when acid-base environment of bulk solution was changed. The ion penetrability in neutral and weak acid solution is stronger than that in alkaline and in strong acid solutions.

The conductance G_b of effective separation layer is the most important parameter for the permeability of ions through membranes, this is because this parameter is closely related to the number of ions in the separation layer. The Born solvation energy barrier, ΔW, is the most important parameter for the selectivity of ions through membranes, because $\triangle$W can categorize the type of electrolyte through the membrane.

This study also shows that the dielectric analysis method adopted in this article is valid and useful for probing the internal information, especially electrical character, of the membrane/solution system. Though the information on ion penetrability and selectivity of NF membrane obtained from dielectric analysis has not yet to be validated experimentally in actual membrane process, the inner structural and electrical parameters of membrane can hardly be acquired from other individual methods. Therefore, at this point, the present method perhaps can provide some enlightenment for solving the problems that are always encountered in complex systems and is still expected to be applied to more membrane/solution systems.

Acknowledgment

Financial supports of this work by the National Natural Science Foundation of China (Nos: 21173025, 20976015) are gratefully acknowledged.

References

[1] N. Hilal, H. A1-Zoubi, N.A. Darwish, A.W. Mohammad, M. Abu Arabi, Desalination 170 (2004) 281–308.
[2] A.E. Yaroshchuk, A.L. Makovetskiy, Y.P. Boiko, E.W. Galinker, J. Membr. Sci. 172 (2000) 203–221.
[3] W.R. Bowen, J.S. Welfoot, Chem. Eng. Sci. 57 (2002) 1393–1407.
[4] Cao Van Chung, Ngo Quoc Buu, Nguyen Hoai Chau, Sci. Technol. Adv. Mater. 6 (2005) 246–250.
[5] Jesus. Garcia-Aleman, James.M. Dickson, J. Membr. Sci. 239 (2004) 163–172.
[6] T.K. Dey, V. Ramachandhran, B.M. Misra, Desalination 127 (2000) 165–175.
[7] M.J. Rosa, M.N. de Pinho, J. Membr. Sci. 89 (1994) 235–243.
[8] J. Schaep, B. Van der Bruggen, C. Vandecasteele, D. Wilms, Separ. Purif. Technol. 14 (1998) 155–162.
[9] A.E. Yaroshchuk, Adv. Colloid Interface Sci. 85 (2000) 193–230.
[10] A.E. Childress, M. Elimelech, Environ. Sci. Technol. 34 (2000) 3710–3716.
[11] L. Ballinas, C. Torras, V. Fierro, R. Garcia-Valls, J. Phys. Chem. Solids 65 (2004) 633–637.
[12] M. Khayet, Appl. Surf. Sci. 238 (2004) 269–272.
[13] K.C. Khulbe, F. Hamad, C. Feng, T. Matsuura, M. Khayet, Desalination 161 (2004) 259–262.
[14] Mathias Erns, Alexander Bismarck, Jürgen Springer, Martin Jekel, J. Membr. Sci. 165 (2000) 251–259.
[15] J.M.M. Peeters, M.H.V. Mulder, H. Strathmann, Colloids Surf. A: Physicochem. Eng. Aspects 150 (1999) 247–259.
[16] Maria Diná Afonso, Georg Hagmeyer, Rolf Gimbel, Sep. Purif. Technol. 22–23 (2001) 529–541.
[17] Benjamin D. Fitz, Jovan Mijovic, J. Phys. Chem. B 104 (2000) 12215–12223.
[18] K. Asami, Prog. Polym. Sci. 27 (2002) 1617–1659.
[19] T. Osaki, A. Tanioka, J. Colloid Interface Sci. 253 (88–93) (2002) 94–102.
[20] T.C. Chilcott, M. Chan, L. Gaedt, T. Nantawisarakul, A.G. Fane, H.G.L. Coster, J. Membr. Sci. 195 (153–167) (2002) 169–180.
[21] H.G.L. Coster, T.C. Chilcott, A.C.F. Coster, Bioelectrochem. Bioenerg. 40 (1996) 79–98.
[22] J.M. Kavanagh, S. Hussain, T.C. Chilcott, H.G.L. Coster, Desalination 236 (2009) 187–193.
[23] J.-S. Park, T.C. Chilcott, H.G.L. Coster, S.-H. Moon, J. Membr. Sci. 246 (2005) 137–144.
[24] Hong-Joo Lee, Min-Kyoung Hong, Sang-Don Han, Joonmok Shim, Seung-Hyeon Moon, J. Membr. Sci. 325 (2008) 719–726.
[25] H.G.L. Coster, J.R. Smith, Biochim. Biophys. Acta 372 (1974) 151–164.
[26] J.S. Park, T.C. Chilcott, H.G.L. Coster, S.-H. Moon, J. Membr. Sci. 246 (15) (2005) 137–144.
[27] O. Kedem, A. Katchalsky, Trans. Faraday Soc. 59 (1963) 1941.
[28] G. Jonsson, J. Benavente, J. Membr. Sci. 69 (1992) 29.
[29] A. Cañas, M.J. Ariza, J. Benavente, J. Membr. Sci. 183 (2001) 135–146.
[30] K. Kiyohara, K.S. Zhao, K. Asaka, T. Hanai, Jpn. J. Appl. Phys. 29 (1990) 1751–1756.
[31] K. Asaka, J. Membr. Sci. 50 (1990) 153.
[32] Y.H. Li, K.S. Zhao, J. Colloid Interface Sci. 276 (2004) 68–76.
[33] Kongshuang Zhao, Yuhong Li, J. Phys. Chem. B 110 (2006) 2755–2763.
[34] K.W. Wagner, Arch. Elektrotech. (Berlin) 2 (1914) 371–387.
[35] T. Hanai, H.Z. Zhang, K. Sekine, K. Asaka, K. Asami, Ferroelectrics 86 (1988) 191–204.
[36] Daniele Vezzani, Serena Bandini, Desalination 149 (2002) 477–483.
[37] M.S. Hall, V.M. Starov, D.R. Lloyd, J. Membr. Sci. 128 (1997) 23–37.
[38] G. Hagmeyer, R. Gimbel, Desalination 117 (1998) 247–256.
[39] W.R. Bowen, J.S. Welfoot, Chem. Eng. Sci. 57 (2002) 1121–1137.
[40] J. Israelachvili, Intermolecular and Surface Forces, 2nd ed., Academic Press, London, 1991.
[41] M. Boström, B.W. Ninham, Biophys. Chem. 114 (2005) 95–101.
[42] K. Asami, A. Irimajiri, T. Hanai, N. Koizumi, Bull. Inst. Chem. Res., Kyoto Univ. 51 (1973) 231.
[43] T. Hanai, in: P. Sherman (Ed.), Emulsion Science, Academic, New York, 1968.
[44] K.S. Cole, R.H. Cole, J. Chem. Phys. 9 (1941) 341–351.
[45] Johan. Schaep, Bart Van der Bruggen, et al., Sep. Purif. Technol. 14 (1998) 155–162.
[46] G. Bargeman, J.M. Vollenbroek, J. Straatsma, C.G.P.H. Schroën, R.M. Boom, J. Membr. Sci. 247 (2005) 11–20.
[47] E.R. Nightingale Jr., J. Phys. Chem. 63 (1959) 1381–1387.
[48] Andriy E. Yaroshchuk, Desalination 149 (2002) 423–428.
[49] Hee-Tak Kim, Jung-Ki Park, Kew-Ho Lee, J. Membr. Sci. 115 (1996) 207–215.
[50] Margarida Ribau Teixeira, Maria João Rosa, Marianne Nyström, J. Membr. Sci. 265 (2005) 160–166.